Functionalized Mesoporous Cross-Linked Polymer As Efficient Host for Loading Gold Nanoparticles and Its Electrocatalytic Behavior for Reduction of H 2 O 2

4 AUTHORS, INCLUDING:

Debraj Chandra
Niigata University
39 PUBLICATIONS **532** CITATIONS

SEE PROFILE

C Retna Raj
IIT Kharagpur
91 PUBLICATIONS **3,204** CITATIONS

SEE PROFILE

Asim Bhaumik
Indian Association for the Cultivation of Sci…
294 PUBLICATIONS **4,662** CITATIONS

SEE PROFILE

Functionalized Mesoporous Cross-Linked Polymer As Efficient Host for Loading Gold Nanoparticles and Its Electrocatalytic Behavior for Reduction of H₂O₂

Debraj Chandra,[†] Bikash Kumar Jena,[‡] C. Retna Raj,*,[‡] and Asim Bhaumik*,[†]

Department of Materials Science and Centre for Advanced Materials, Indian Association for the Cultivation of Science, Jadavpur, Kolkata - 700 032, India, Department of Chemistry, Indian Institute of Technology, Kharagpur 721 302, India

A new all-organic mesoporous cross-linked polymer (MCP-1) has been synthesized hydrothermally through in situ aqueous-phase radical polymerization of acrylic acid in the presence of a supramolecular assembly of cationic surfactant cetyltrimethylammonium bromide (CTAB) as the structure-directing agent (SDA) and *N,N*-methylene-bis-acrylamide as a cross-linker. After successful removal of the SDA molecules through solvent extraction, gold nanoparticles (GNPs) stabilized in the presence of positively charged tris(hydroxymethyl) aminomethane (TRIS) have been loaded into the mesopores through the electrostatic interaction with the –COO⁻ groups existing at the surface of the mesopores. Powder X-ray diffraction (XRD), high-resolution transmission electron microscopy (HRTEM), field-emission scanning electron microscopy/energy-dispersive spectrometry (FESEM-EDS), N₂ sorption, ¹³C cross-polarization magic angle spinning (¹³C CPMAS) NMR, Fourier transform infrared spectroscopy, and UV–visible spectroscopic analysis were carried out to characterize the solid mesoporous materials before and after GNP loading. XRD and HRTEM analyses demonstrated the existence of mesopores and a wormholelike disordered nanostructure. N₂ sorption data revealed good Brunauer–Emmett–Teller surface areas together with type IV isotherms for the MCP-1 samples. FESEM and UV–visible spectral measurements confirm the loading of GNPs. The electrode modified with GNP-loaded MCP-1 can efficiently catalyze the reduction of H₂O₂.

Introduction

Mesoporous materials have been synthesized by employing the 2D or 3D supramolecular assembly[1] formed by the liquid crystalline array of surfactant molecules as a core, around which the solid inorganic matrixes are formed. Subsequent removal of the surfactant molecules from this composite can generate mesoporosity according to the size of the self-assemblies in those solid materials. This soft templating approach for the synthesis of ordered nanostructure materials has been extensively practiced since the first synthesis of ordered mesoporous silica, MCM-41/48, by Mobil researchers in 1992.[2] Mesoporous materials invented so far have attracted widespread attention for adsorption, exchanger, and catalysis purposes and applications as hosts for the synthesis of nanomaterials, as they usually have very high surface area and tunable pore diameters vis-à-vis related microporous materials.[3] Besides silica-based materials, the transition-metal-containing mesoporous molecular sieves have huge potential in the fields of catalysis,[4–6] optical,[7] electronic,[8] magnetic,[9] and sensor applications.[10] In this context, meso-

porous carbons[11] synthesized by pyrolyzing the mesophase pitch and resins have attracted considerable attention in recent times. Compared to the numerous examples of inorganic and organic–inorganic hybrid mesoporous materials,[12–14] very few research works have been carried out on purely organic porous nanostructured materials[15] devoid of the pyrolysis

* Authors to whom correspondence should be addressed. E-mail: crraj@chem.iitkgp.ernet.in (C.R.R.); msab@mahendra.iacs.res.in (A.B.).
  [†] Indian Association for the Cultivation of Science.
  [‡] Indian Institute of Technology.

 (1) Huo, Q.; Margolese, D. I.; Stucky, G. D *Chem. Mater.* **1996,** *8,* 1147–1160.
 (2) Kresge, C. T.; Leonowicz, M. E.; Roth, W. J.; Vartuli, J. C.; Beck, J. S. *Nature* **1992,** *359,* 710–712.
 (3) Szostak, R. *Molecular Sieves: Principles of Synthesis and Identification*; Van Nostrand Reinhold, New York, 1989.
 (4) Goa, Y.; Wu, P.; Tatsumi, T. *J. Phys. Chem. B* **2004,** *108,* 8401–8411.
 (5) Bhaumik, A.; Tatsumi, T. *J. Catal.* **2000,** *189,* 31–39.
 (6) Bhaumik, A.; Samanta, S.; Mal, N. K. *Microporous Mesoporous Mater.* **2004,** *68,* 29–35.
 (7) (a) Frindell, K. L.; Tang, J.; Harreld, J. H.; Stucky, G. D. *Chem. Mater.* **2004,** *16,* 3524–3532. (b) Sanchez, C.; Lebeau, B.; Chaput, F.; Boilot, J. P. *Adv. Mater.* **2003,** *15,* 1969–1994.
 (8) Lu, D.; Katou, T.; Uchida, M.; Kondo, J. N.; Domen, K. *Chem. Mater.* **2005,** *17,* 632–637.
 (9) Jiao, F.; Harrison, A.; Jumas, J.-C.; Chadwick, A. V.; Kockelmann, W.; Bruce, P. G. *J. Am. Chem. Soc.* **2006,** *128,* 5468–5474.
(10) Yamada, T.; Zhou, H. S.; Uchida, H.; Tomita, M.; Ueno, Y.; Ichino, T.; Honma, I.; Asai, K.; Katsube, T. *Adv. Mater.* **2002,** *14,* 812–815.
(11) (a) Liang, C.; Dai, S. *J. Am. Chem. Soc.* **2006,** *128,* 5316–5317. (b) Gierszal, K. P.; Jaroniec, M. *J. Am. Chem. Soc.* **2006,** *128,* 10026–10027. (c) Valkama, S.; Nykänen, A.; Kosonen, H.; Ramani, R.; Tuomisto, F.; Engelhardt, P.; Ten Brinke, G.; Ikkala, O.; Ruokolainen, J. *Adv. Funct. Mater.* **2007,** *17,* 183–190.
(12) (a) Inagaki, S.; Guan, S.; Fukushima, Y.; Ohsuna, T.; Terasaki, O. *J. Am. Chem. Soc.* **1999,** *121,* 9611–9614. (b) Asefa, T.; MacLachlan, M. J.; Coombs, N.; Ozin, G. A. *Nature* **1999,** *402,* 867–871.
(13) (a) Melde, B. J.; Holland, B. T.; Blanford, C. F.; Stein, A. *Chem. Mater.* **1999,** *11,* 3302–3308. (b) Sayari, A.; Hamoudi, S. *Chem. Mater.* **2001,** *13,* 3151–3168. (c) Anwander, R. *Chem. Mater.* **2001,** *13,* 4419–4438.
(14) (a) Bhaumik, A.; Kapoor, M. P.; Inagaki, S. *Chem. Commun.* **2003,** 470–471. (b) Nakajima, K.; Tomita, I.; Hara, M.; Hayashi, S.; Domen, K.; Kondo, J. N. *Adv. Mater.* **2005,** *17,* 1839–1842. (c) Kimura, T. *Chem. Mater.* **2003,** *15,* 3742–3744.

step necessary for the synthesis of mesoporous carbons. The organic mesoporous material thus produced can carry functional organic groups at the surface of the mesopores, which may have many unique potential applications as catalysts and hosts for stabilizing nanoparticles in a solid matrix.

Development of an efficient electrochemical interface for the sensing of industrially and pharmaceutically important analytes has received considerable attention. Various approaches have been employed for the modification of electrode surfaces.[16,17] Because the nanosized materials are known to function as efficient catalysts, modification of the electrode surface with nanosized materials is of recent interest.[18–21] The coinage metal particles have been extensively used as a catalyst for the oxidation of methanol, reduction of oxygen, and so forth.[22,23] The catalytic activity of these metal particles depends on the size, morphology, and choice of support used to confine the nanoparticles.[24,25] The mesoporous materials could be explored as a host or a matrix[26] to confine the nanosized metal particles. The mesoporous materials such as silica, titania, zirconia, and so forth have been used as a catalyst/enzyme support to investigate the catalytic properties of different metal particles[27,28] and for stabilizing the metal particles.[29,30] Thus, mesoporous materials with a pore diameter on the nanometer scale and large internal surface area can be used as ideal catalyst supports.

Herein, we first report the synthesis of all-organic mesoporous polymers by using the supramolecular assembly of cationic surfactants in situ during the radical polymerization of acrylic acid (AA) with a cross-linker under hydrothermal conditions. This is followed by the removal of the structure-directing agent (SDA) by solvent extraction to make the all-organic framework mesoporous material. The material thus

synthesized was found to have –CO_2H groups and has been successfully used for the loading of positively charged nanosized Au particles (GNPs). The electrochemical and electrocatalytic behaviors of this hybrid material (GNP-MCP-1) have been examined. This GNP-MCP-1 material shows good electrocatalytic activity toward H_2O_2.

Experimental Section

Materials. Acrylic acid (monomer), *N*,*N*,*N*′,*N*′-tetramethyl-ethylenediamine (TEMED, promoter), *N*,*N*-methylene-bis-acrylamide (BA, cross-linker), and ammonium persulfate (APS, initiator) were obtained from Loba Chemie, and $HAuCl_4$, tetraethyl orthosilicate (TEOS), tetramethylammonium hydroxide (25% aqueous), and tris(hydroxymethyl) aminomethane (TRIS) were obtained from Sigma-Aldrich and used as received. Hydrogen peroxide (30%) was obtained from E-Merck. All other chemicals, unless mentioned otherwise, used in this investigation were of analytical grade. All the solutions were prepared with Millipore water.

Instrumentation. Powder X-ray diffraction (XRD) patterns of different samples were analyzed with a Seifert P 3000 X-ray diffraction unit using Ni-filtered Cu Kα ($\lambda = 1.54$ Å) radiation. N_2 adsorption/desorption isotherms of the sample were recorded on a Quantachrome Autosorb 1-C, at 77 K. Prior to the measurement, the sample was degassed at 373 K for 8 h under high vacuum conditions. Transmission electron microscopy (TEM) images of the mesoporous polymer and Au nanoparticles were obtained using a JEOL JEM 2010 transmission electron microscope operating at 200 kV. The samples were prepared by dropping 2 μL of colloidal solution onto carbon-coated copper grids. Scanning electron microscopic measurements were performed with a JEOL JEM 6700F field-emission scanning electron microscope (FESEM). UV–visible absorption spectral measurements were carried out using a Shimadzu UV-1601 double-beam spectrophotometer. The UV–visible diffuse reflectance spectra (DRS) of MCP-1 and GNP-MCP-1 hybrid materials were measured with a Shimadzu UV-2401 PC spectrophotometer using $BaSO_4$ as a background standard. Thermogravimetry (TGA) and differential thermal analyses (DTA) of the samples were carried out on a TA instruments Q600 DSC/TGA thermal analyzer. Electrochemical measurements were performed using a two-compartment three-electrode cell with a glassy carbon (GC) working electrode, a Pt wire auxiliary electrode, and a Ag/AgCl (3 M NaCl) reference electrode. Cyclic voltammograms were recorded using a computer-controlled CHI643B electrochemical analyzer. The impedance analysis was carried out using the program EQUIVALENT CIRCUIT written by B.A. Boukamp (University of Twente). The impedance at the formal potential of the redox couple, which was superimposed on 5 mV root-mean-square sinusoidal potential modulations, was measured in the frequency range of 10 mHz to 100 kHz. The impedance spectra are plotted in the complex plane diagram [Nyquist plot (real impedance (Z') vs imaginary impedance (Z'')]. The electrophoresis measurement was carried out with a Prince CE system (Prince Technologies, Netherlands) equipped with an autosampler, a LAMBDA 1010 variable wavelength UV–visible absorbance detector (Bischoff, Leonberg, Germany), and an in-built temperature control system. Data were collected using a personal computer in conjunction with DAX 7.0 data acquisition and analysis software. The injection was performed in a phosphate buffer solution (PBS) using the pressure method (15 mbar, 2s) under a constant potential of 15 kV. Methanol was used as a neutral marker.

Synthesis of MCP-1. MCP-1 was synthesized through the aqueous-phase polymerization of acrylic acid under hydrothermal conditions by using APS as an initiator and BA as a cross-linker. In a typical synthesis, 0.01 mol (3.64 g) of cetyltrimethylammonium

(15) (a) Mao, H.; Hillmyer, M. A. *Soft Matter* **2006**, *2*, 57–59. (b) Qiao, W. M.; Song, Y.; Hong, S. H.; Lim, S. Y.; Yoon, S. H.; Korai, Y.; Mochida, I. *Langmuir* **2006**, *22*, 3791–3797. (c) Lu, Y. *Angew. Chem., Int. Ed.* **2006**, *45*, 7664–7667. (d) Zhang, F.; Meng, Y.; Gu, D.; Yan, Y.; Chen, Z.; Tu, B.; Zhao, D. *Chem. Mater.* **2006**, *18*, 5279–5288. (e) Liu, C.; Li, L.; Song, H.; Chen, X. *Chem. Commun.* **2007**, 757–759. (f) Nandi, M.; Gangopadhyay, R.; Bhaumik, A. *Microporous Mesoporous Mater.* **2007** [Online] DOI:, 10.1016/j. micromeso. 2007.04.049.
(16) Katz, E.; Willner, I. *Angew. Chem., Int. Ed.* **2004**, *43*, 6042–6108.
(17) Murray, R. W. In *Electroanalytical Chemistry*; Bard, A. J., Ed.; Marcel Dekker: New York, 1984; p 191.
(18) Raj, C. R.; Jena, B. K. *Chem. Commun.* **2005**, 2005–2007.
(19) Jena, B. K.; Raj, C. R. *Chem.—Eur. J.* **2006**, *12*, 2702–2708.
(20) Jena, B. K.; Raj, C. R. *Anal. Chem.* **2006**, *78*, 6332–6339.
(21) Jena, B. K.; Raj, C. R. *Langmuir* **2007**, *23*, 4064–4070.
(22) Zhong, C.-J.; Maye, M. M. *Adv. Mater.* **2001**, *13*, 1507–1511.
(23) El-Deab, M. S.; Ohsaka, T. *Electrochem. Commun.* **2002**, *4*, 288–292.
(24) Narayanan, R.; El-Sayed, M. A. *J. Phys. Chem. B* **2005**, *109*, 12663–12676.
(25) (a) Valden, M.; Lai, X.; Goodman, D. W. *Science* **1998**, *281*, 1647–1650. (b) Haruta, M. *Catal. Today* **1997**, *36*, 153–166.
(26) Meynen, V.; Cool, P.; Vansant, E. F.; Kortunov, P.; Grinberg, F.; Kärger, J.; Mertens, M.; Lebedev, O. I.; Van Tendeloo, G. *Microporous Mesoporous Mater.* **2007**, *99*, 14–22.
(27) (a) Mukhopadhyay, K.; Phadtare, S.; Vinod, V. P.; Kumar, A.; Rao, M.; Chaudhari, R. V.; Sastry, M. *Langmuir* **2003**, *19*, 3858–3863. (b) Bandyopadhyay, M.; Korsak, O.; van den Berg, M. W. E.; Grunert, W.; Birkner, A.; Li, W.; Schuth, F.; Gies, H. *Microporous Mesoporous Mater.* **2006**, *89*, 158–163.
(28) Ilieva, L.; Sobczak, J. W.; Manzoli, M.; Su, B. L.; Andreeva, D. *Appl. Catal., A* **2005**, *291*, 85–92.
(29) Yang, C.-m.; Liu, P.-h.; Ho, Y.-f.; Chiu, C.-y.; Chao, K.-j. *Chem. Mater.* **2003**, *15*, 275–280.
(30) Aprile, C.; Abad, A.; García, H.; Corma, A. *J. Mater. Chem.* **2005**, *15*, 4408–4413.

bromide (CTAB) and 0.04 mol (2.88 g) of acrylic acid were dissolved in 30 mL of water. This was followed by the addition of 0.01 mol (1.54 g) of BA to this solution. Finally, 0.02 mol (4.56 g) of APS and 0.01 mol (1.16 g) of TEMED dissolved in 20 mL of water were added into the solution under vigorous stirring. This was followed by the slow addition of NaOH (25% aqueous) under constant stirring. After 1 h, the resultant solution was autoclaved at 348 K for 3 days under static conditions. The pH's for different gels were ca. 7.0–8.0. The resultant precipitate was filtered and washed with deionized water, yielding mesoporous polymer MCP-1. The surfactant was removed from these as-synthesized materials by extracting 1.0 g of the as-made material with 0.5 g of acetic acid in 50 mL of water at 298 K for 4 h under stirring twice, followed by the extraction of 0.5 g of this acid-extracted sample with a solution containing 1.75 g of NH_4F in 50 mL of water for 3 h. We have prepared three different samples with different molar ratios of the monomer to the cross-linker, 2:1, 4:1, and 6:1. Since the sample synthesized with a 4:1 molar ratio of AA/BA has the highest XRD peak intensity, which has been retained after the removal of the CTAB molecules, this MCP-1 sample has been characterized in detail and used as a host for loading gold nanoparticles.

Synthesis of Colloidal Au Nanoparticles. In a typical synthesis, 0.1 mL of an aqueous solution of 1% $HAuCl_4$ was added to 10 mL of water containing 0.5 mM TRIS and was stirred for 2 min. Then, 0.25 mL of an aqueous solution of $NaBH_4$ (0.08%) was added dropwise under stirring. The stirring was continued for another 10 min, and the resulting nanocolloid was stored at 4 °C.

Preparation of GNP-MCP-1 Hybrid Material. A total of 50 mg of MCP-1 was dispersed in 10 mL of TRIS-stabilized GNPs and stirred for 1 h at room temperature. The color of the colloidal nanoparticles gradually disappeared while stirring. The supernatant solution was colorless after 1 h of stirring at room temperature, whereas the color of MCP-1 changed to purple, indicating the loading of GNPs onto the surface of MCP-1. After centrifugation, purple-colored hybrid material (GNP-MCP-1) was obtained. This hybrid material was washed further with copious amounts of water and dried at room temperature. The loading of GNP onto MCP-1 was further confirmed by spectral measurements.

Preparation of Silica Sol. The TEOS sol was prepared by dissolving 0.4 mL of TEOS and 0.6 mL of ethanol in 0.2 mL water (as 0.1 M HCl) and stirring the mixture vigorously for 30 min, and this sol was stored at 4 °C.

Fabrication of Electrode. GC electrodes (0.07 cm^2) were used as the substrate for fabrication of the GNP-MCP-1 hybrid electrode. First, the GC electrodes were polished well with fine emery paper and an alumina (0.05 μm) slurry and then were sonicated in Millipore water for 10–15 min. The polished electrode was rinsed extensively with Millipore water and dried at room temperature. A total of 5 mg of GNP-MCP-1 or MCP-1 material was suspended in 1 mL of the TEOS sol and stirred for ∼5 min. A total of 15 μL of the suspension was cast over the GC electrode and allowed to dry at room temperature. For the control experiments, GC electrodes were modified with 15 μL of TEOS sol and dried at room temperature. Hereafter, the GNP-MCP-1 and MCP-1 materials and TEOS sol modified electrodes will be referred to as GC/GNP-MCP-1, GC/MCP-1, and GC/TEOS electrodes, respectively. All of the experiments were carried out in an argon atmosphere.

Results and Discussion

Characterization of MCP-1 Material. In Figure 1, the low-angle XRD patterns of the as-synthesized, extracted, and subsequent gold-loaded forms of MCP-1 sample are shown. A single low-angle peak was observed for all of the samples
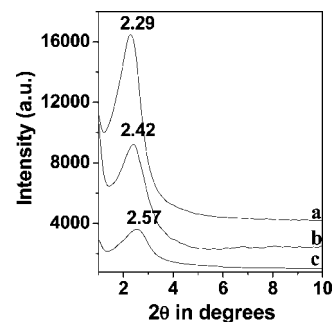

Figure 1. Powder XRD patterns of (a) as-synthesized and (b) extracted mesoporous MCP-1 and GNP-MCP-1 (c).
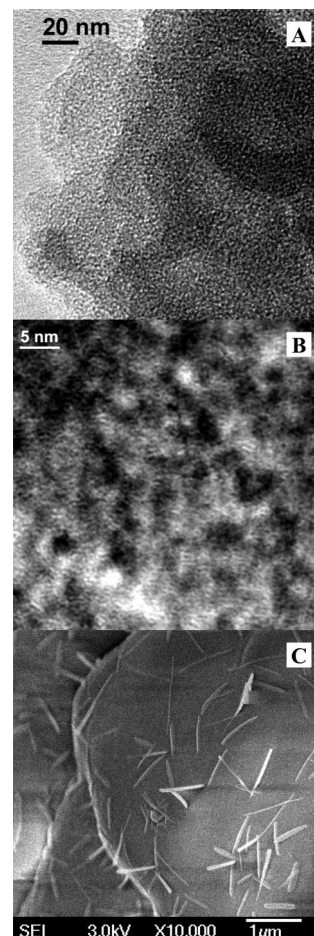
Figure 2. Low magnification (A) and high magnification (B) HRTEM and FESEM (C) images of MCP-1 material.

with no detectable peak at a high angle, which indicates that the samples are mesostructured, but there is no short- or long-range ordering. The extracted sample showed relatively weaker intensity and a broader peak width (Figure 1b) in comparison to the as-synthesized one (Figure 1a). This result suggested that the nanostructure had been restored after the removal of the surfactant. However, the arrangement of the pores became more disordered after the removal of SDA. The powder XRD pattern of the gold-loaded mesoporous sample (GNP-MCP-1, Figure 1c) also suggested the existence of a mesophase. The high-resolution transmission electron microscopy (HRTEM) images of the as-synthesized sample are shown in Figure 2A and 2B. These images confirm the formation of low-electron-density spherical spots of ca. 2.5
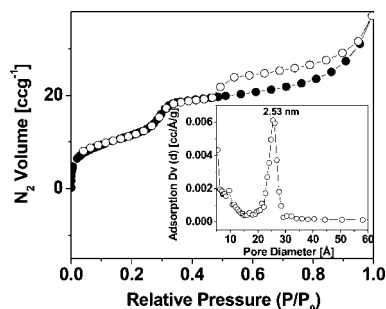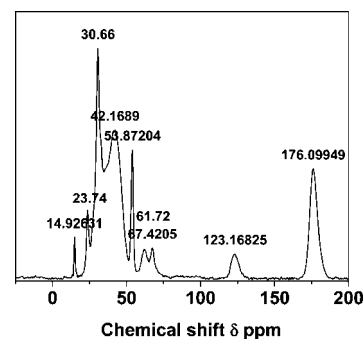
Figure 3. N_2 adsorption/desorption isotherms of template-free MCP-1. Adsorption points are marked by filled circles and desorption points by empty circles. BJH pore size distribution is shown in the inset.
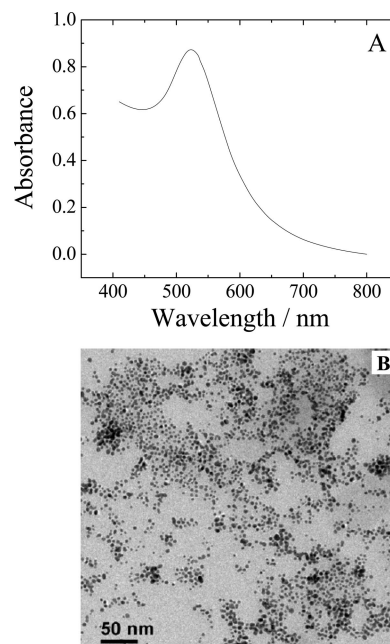
nm in diameter. These high-resolution images suggested wormholelike disordered arrangements of pores. Thus, from the XRD pattern and the TEM image analysis, we could conclude that this mesoporous MCP-1 material has a disordered wormholelike structure. Supramolecular-templated mesoporous silicas, for example, MSU-1[32] and so forth, exhibited similar common pore center-to-center correlation lengths, characteristic of a wormholelike structure. In Figure 2C, a FESEM image of MCP-1 is shown. From Figure 2C, it is clear that the material has a nanotube-like morphology. Interestingly, these nanosized tubes are 150–300 nm long and 30–50 nm wide.

In Figure 3, the N_2 adsorption–desorption isotherms of the MCP-1 material are shown. This isotherm is a typical type IV isotherm, characteristic of mesoporous solids.[1,2] Very rarely, all-organic framework functionalized material could exhibit this type IV isotherm. A sharp increase of N_2 uptake corresponding to the capillary condensation was observed in the mesopore region together with a large hysterisis, as usually observed for inorganic framework mesoporous materials.[33] The Brunauer–Emmett–Teller (BET) surface area for this sample was 56 m^2g^{-1}. Porous organics synthesized from phenols and formaldehyde also exhibited a similar range of surface areas. The pore-size distribution of this sample estimated by using the Bopp–Jancso–Heinzinger (BJH) method suggested a narrow distribution with maxima at 2.53 nm. The average pore diameter estimated from the TEM image analysis also agrees well with this value.

The quantitative determination of the content of poly-(acrylic acid) in surfactant-free MCP-1 was estimated by using TGA and DTA in the presence of a N_2 flow. The TGA and DTA analyses of the MCP-1 sample show a first weight loss at up to 373 K due to desorption of the physisorbed water (ca. 8.0 wt %; Supporting Information). This is followed by two sharp decreases in the weight between temperatures 453 and 673 K, which could be attributed to the loss of acrylic acid and bis-acrylamide fragments present in MCP-1. A considerable endothermic peak in the DTA plot centered at 558 K suggested that most of the organic fragment was decomposed at that point. A total loss of ca.

(31) Yang, C. -M.; Sheu, H.-S.; Chao, K. -J. *Adv. Funct. Mater.* **2002**, *12*, 143–148.
(32) Bagshaw, S. A.; Prouzet, E.; Pinnavaia, T. J. *Science* **1995**, *269*, 1242–1244.
(33) de Araujo, C. C.; Zhang, L.; Eckert, H. *J. Mater. Chem.* **2006**, *16*, 1323–1331.

Figure 4. ^{13}C MAS NMR spectra of the mesoporous MCP-1.

Figure 5. (A) UV–visible spectra and (B) TEM image obtained for GNPs.

73.6 wt % was observed in this temperature range. Above this temperature, a further gradual weight loss occurred, which could be attributed to the complete conversion of the material into nanostructure carbon.
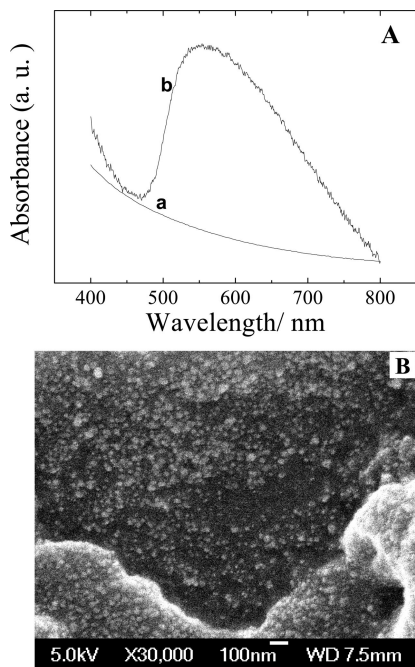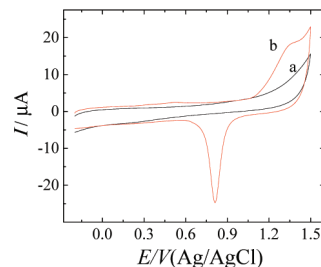
In Figure 4, the ^{13}C cross-polarization magic angle spinning (CPMAS) NMR spectra of the mesoporous polymer MCP-1 is shown. A sharp peak at 30.7 ppm together with mild peaks at 14.9, 23.7, 42.1, 53.8, 123.1, and 176.1 ppm were observed, whereas the characteristic signals of residual acrylic acid and BA molecules at 115.8 and 132.6 ppm were very poor. This result suggested that acrylic acid and BA moieties have undergone polymerization to give a cross-linked polymeric framework in the mesoporous MCP-1 sample.

Characterization of Colloidal Au Nanoparticles. The UV–visible spectrum of TRIS-stabilized GNP shows a strong absorption band corresponding to the surface plasmon resonance at ∼520 nm (Figure 5A). The size and shape of the nanoparticles were examined by HRTEM (Figure 5B). The TEM image obtained shows that the nanoparticles have a spherical shape with an average size of 5 ± 1 nm. It is interesting to note that almost all of the nanoparticles are the same size. The concentration of nanoparticles was estimated[34] from the size and molar

Figure 7. Cyclic voltammogram for (a) GC/MCP-1 and (b) GC/GNP-MCP-1 electrodes in 0.1 M H_2SO_4. Scan rate 100 mV/s.

Figure 6. (A) UV–visible diffuse reflectance spectra of (a) MCP-1 and (b) GNP-MCP-1 hybrid material and (B) FESEM image of GNP-MCP-1 hybrid material.

volume of gold (10.2 mL/mol) and was 96 nM. Since the pK_a of TRIS is 8.075, the amine groups are protonated in neutral pH[35] and the GNP are expected to be positively charged under the experimental conditions used in the investigation, due to the adsorption of TRIS on the surface of GNP. This has been confirmed by electrophoresis measurements (Supporting Information).

Characterization of GNP-MCP-1 Hybrid Material. As described earlier, MCP-1 is negatively charged, with –COO⁻ groups of the monomer acrylate at the surface, and hence a possible electrostatic interaction is expected with the positively charged GNPs. The electrostatic effect strongly favors the loading of GNPs on the surface of the MCP-1. The UV–visible diffuse reflectance spectrum of MCP-1 does not show any characteristic band, whereas the GNP-MCP-1 hybrid material shows an absorption band at ∼550 nm corresponding to the GNP on the surface (Figure 6A). The SP band observed for the nanoparticles on the surface of MCP-1 is red-shifted (∼30 nm) with respect to the colloidal nanoparticles, and it can be attributed to the change of the refractive index[36] and the aggregation of GNPs on the surface of MCP-1.[37] It is well-documented in the literature that the electrostatic effect induces the aggregation of nanoparticles.[38] It should be mentioned here that the GNP loaded onto MCP-1 does not leach and is strongly bound to the surface. The strong binding was confirmed by soaking the GNP-MCP-1 material in PBS for ∼24 h, and the absorption spectrum of

the supernatant solution was measured after 24 h (Supporting Information). No characteristic band was observed for the supernatant solution, confirming that GNP does not leach from the surface of MCP-1. In order to examine the nature of the nanoparticles on the surface, FESEM measurements have been performed. Figure 6B shows the FESEM image obtained for the GNP-MCP-1 material. The GNPs are distributed throughout the surface of MCP-1 and have a size distribution between 10 and 25 nm. Moreover, the existence of aggregated nanoparticles on the surface is clearly seen, which is in agreement with the DRS results. After gold loading, the low-angle peak of MCP-1 was further shifted to a higher angle (Figure 1c), suggesting a decrease in the pore-center-to-pore-center lengths. The wide-angle XRD pattern obtained for the GNP-MCP-1 material exhibits four peaks corresponding to the (111), (200), (220), and (311) planes of a face-centered-cubic lattice of Au (Supporting Information). The peak corresponding to the (111) plane is very intense; the ratio between the intensities of (200) and (111) diffraction peaks is much lower than the conventional value, demonstrating that the (111) plane is the predominant orientation.

Figure 7 shows the cyclic voltammograms obtained for the GC/MCP-1 and GC/GNP-MCP-1 electrodes in 0.1 M H_2SO_4. A broad oxidation wave in the potential range from 1.2 to 1.5 V and a reduction peak at ∼0.845 V, corresponding to the formation of surface oxides and their reduction, were observed. Such a voltametric response was not observed for the GC/MCP-1 electrode (Figure 7a), revealing that the voltametric features of the GC/GNP-MCP-1 electrode are due to the presence of GNPs. The surface area of GNPs on the hybrid material was calculated from the charge consumed during the reduction of surface oxides using the reported value of 400 $\mu C/cm^2$ for a clean Au electrode[39] and was 0.0361 cm^2.

In order to further understand the nature of the GC/GNP-MCP-1 electrode, the voltammetric and impedance responses of the hybrid material toward the redox couple $Fe(CN)_6^{4-/3-}$ were examined. The TEOS-sol-modified electrode showed a sluggish voltammetric response for $Fe(CN)_6^{4-/3-}$ (Figure 8). The peak-to-peak separation (ΔE_p) is very large (∼500 mV), indicating that the TEOS on the electrode surface inhibits the electron transfer for the redox reaction. The redox molecule could not permeate through the silicate film on the electrode surface. On the other hand, the GC/MCP-1

(34) Neiman, B.; Grushka, E.; Lev, O. *Anal. Chem.* **2001**, *73*, 5220–5227.
(35) Etz, E. S.; Robinson, R. A.; Bates, R. G. *J. Sol. Chem.* **1973**, *2*, 405–415.
(36) Ung, T.; Liz-Marzan, L. M.; Mulvaney, P. *J. Phys. Chem. B* **2001**, *105*, 3441–3452.
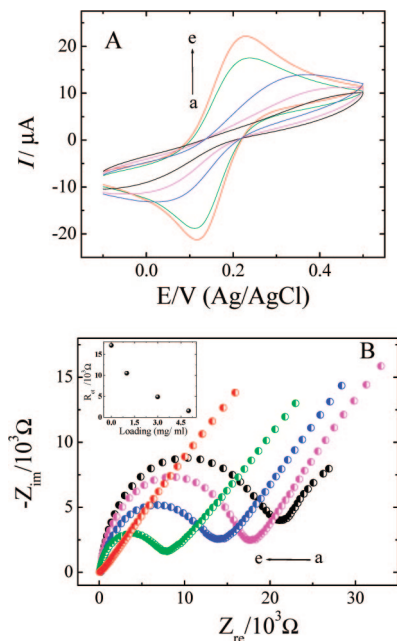(37) Link, S.; El-Sayed, M. A. *J. Phys. Chem. B* **1999**, *103*, 8410–8426.
(38) Shipway, A. N.; Lahav, M.; Gabai, R.; Willner, I. *Langmuir* **2000**, *16*, 8789–8795.

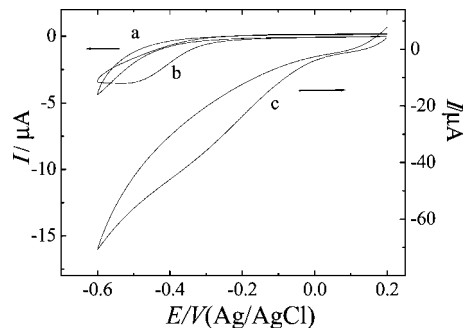(39) (a) Trasatti, S.; Petrii, O. A. *Pure Appl. Chem.* **1991**, *63*, 711–734. (b) Angerstein-Kozlowska, H.; Conway, B. E.; Hamelin, A.; Stoicoviciu, L. *J. Electroanal. Chem.* **1987**, *228*, 429–453.

Functionalized Mesoporous Cross-Linked Polymer

Chem. Mater., Vol. 19, No. 25, 2007 6295

Figure 8. (A) Cyclic voltammograms and (B) Nyquist plots for $Fe(CN)_6^{4-/3-}$ redox couple in 0.1 M KCl illustrating the effect of GNP-MCP-1 hybrid material loading on the electrode surface. (a) MPTS, (b) MCP-1, and (c–e) amount of GNP-MCP-1 loaded (mg/ml): (c) 1, (d) 3, (e) 5, respectively. Inset shows the plot of R_{ct} vs loading of GNP-MCP-1 hybrid material on the electrode surface. Scan rate 100 mV/s.

electrode shows a sluggish voltammetric response with a ΔE_p of ~400 mV. Compared with the GC/TEOS electrode, the GC/MCP-1 electrode shows improved electron transfer kinetics, possibly due to the increase in porosity of the electrode. Very interestingly, the GC/GNP-MCP-1 electrode exhibits a reversible redox response with a ΔE_p value of ~90 mV. The GNPs on the hybrid material tune the electrochemical characteristics of the electrode and favor fast electron transfer kinetics. The voltammetric and impedance responses of the electrode at different loadings of GNP-MCP-1 have been registered to understand the influence of GNPs on the electron transfer reaction. A gradual increase in the peak current with a significant decrease in the ΔE_p value has been noticed as the loading of GNP-MCP-1 hybrid material was increased. The peak current attained a maximum value of 22.8 μA at a 5 mg/mL loading of GNP-MCP-1 on the electrode surface. In the impedance experiments, a gradual decrease in the charge transfer resistance (R_{ct}) while increasing the loading of GNP-MCP-1 was observed (Figure 8B inset), clearly showing that the GNP on MCP-1 facilitates electron transfer for the redox reaction. The increase in the loading of GNP-MCP-1 leads to an increase in the GNP coverage on the electrode surface, which is reflected in a gradual increase in the electron transfer kinetics (a decrease in the ΔE_p and R_{ct} values). Such facilitated electron transfer for the electrodes modified with gold nanoparticle–mesoporous silica and calcium carbonate microsphere–gold nanoparticle composites has been reported in the literature.[40,41]

(40) Cai, W.-Y.; Xu, Q.; Zhao, X.-N.; Zhu, J.-J.; Chen, H.-Y. *Chem. Mater.* **2006**, *18*, 279–284.
(41) Bai, Y.; Yang, H.; Yang, W.; Li, Y.; Sun, C. *Sens. Actuators, B* **2007**, *124*, 179–186.

Figure 9. Cyclic voltammogram obtained for the reduction of H_2O_2 (0.1 mM) on (a) GC/TEOS, (b) GC/MCP-1, and (c) GC/GNP-MCP-1 electrodes in 0.1 M PBS. Scan rate 25 mV/ s.

The GNPs on the surface of MCP-1 achieve good electrical communication with the underlying electrode surface.

Electrocatalytic Reduction H_2O_2. The nanostructured metal particles are known to be an excellent catalyst in different electrochemical reactions.[22,23,42] It has been demonstrated that the chemically and electrochemically synthesized GNPs have excellent activity.[22–24,42] Because the electrochemical detection of H_2O_2 is of great interest in the area of the biosensor and food and pharmaceutical industries,[43] we have examined the electrocatalytic activity of GNP-MCP-1 toward the detection of H_2O_2. Figure 9 illustrates the typical cyclic voltammograms obtained for the reduction of H_2O_2 at the GC/GNP-MCP-1 electrode. The GC/GNP-MCP-1 electrode shows a large anodic wave at about –0.3 V for the reduction of H_2O_2. Such a characteristic voltammetric response was not observed at either the GC/TEOS or GC/MCP-1 electrode in the potential window used. The GC/MCP-1 electrode shows a broad reduction wave for H_2O_2 at about –0.5 V, whereas the GC/TEOS electrode does not show any characteristic peak. The reduction of H_2O_2 on the unmodified GC electrode takes place at >–0.6 V, which is 300 mV more negative than that on the present GC/GNP-MCP-1 electrode. These results reveal that the GNPs on the hybrid material efficiently catalyze the reduction of H_2O_2 at a less negative potential. The voltammetric response is very stable, and a gradual increase in the cathodic current was obtained while increasing the concentration of H_2O_2. The magnitude of the voltammetric current for the reduction of H_2O_2 at a fixed concentration does not change upon repeated sweeps, confirming that the GC/GNP-MCP-1 electrode is highly stable and can be used for repeated measurements. The operational stability of the GC/GNP-MCP-1 electrode was examined by using the same electrode for repeated measurements at different time intervals. The voltammetric current for the reduction of H_2O_2 (25 μM) was measured at a scan rate of 25 mV/s every 5 h for 1 day. The magnitude of the reduction current does not change appreciably during the whole set of experiments, indicating that the electrode is highly stable (Supporting Information).

(42) Li, Y.; Shi, G. *J. Phys. Chem. B.* **2005**, *109*, 23787–23793.
(43) (a) De Mattos, I. L.; Gorton, L.; Ruzgas, T. *Biosens. Bioelectron.* **2003**, *18*, 193–200. (b) Sun, D.; Cai, C.; Li, X.; Xing, W.; Lu, T. *J. Electroanal. Chem.* **2004**, *566*, 415–421. (c) Ferapontova, E.; Gorton, L. *Bioelectrochem.* **2002**, *55*, 83–87.

Conclusions

A new all-organic mesoporous cross-linked polymer MCP-1 has been synthesized hydrothermally through in situ aqueous radical polymerization of acrylic acid and a cross-linker in the presence of CTAB as a SDA. CTAB molecules were removed from this mesoporous material by solvent extraction, and then gold nanoparticles were loaded over its surface. Powder XRD, HRTEM, FESEM-EDS, N_2 sorption, ^{13}C CPMAS NMR, Fourier transform infrared spectroscopy, and UV–visible spectroscopic analysis were carried out to characterize the solid mesoporous materials before and after the loading of GNPs. N_2 sorption data suggested good BET surface areas together with type IV isotherms for MCP-1. Electron microscopic and spectroscopic data confirm the loading of gold nanoparticles on MCP-1. The GNP-MCP-1 hybrid material shows very good electrocatalytic activity toward the reduction of H_2O_2. As the GNP-MCP-1-modified electrode shows high sensitivity toward H_2O_2, it can be successfully used for the development of oxidase-based amperometric biosensors.

Supporting Information Available: TGA and DTA plots for MCP, electropherogram obtained for TRIS-stabilized Au nanoparticles and the neutral marker (methanol), UV-visible absorption spectra of the supernatant solution of GNP-MCP-1 hybrid material and only PBS, wide-angle XRD pattern for GNP-MCP-1 and MCP-1 materials, and a graph illustrating the operational stability of the GC/GNP-MCP-1 electrode towards H_2O_2 (25 BM) in 0.1 M PBS. This material is available free of charge via the internet at http://pubs.acs.org.

CM702259Q